Article

U-Pb Age Dating and Geochemistry of Soft-Sediment Deformation Structure-Bearing Late Cretaceous Volcano-Sedimentary Basins in the SW Korean Peninsula and Their Tectonic Implications

Kyoungtae Ko [1], Sungwon Kim [1,*] and Yongsik Gihm [2]

[1] Geology Division, Korea Institute of Geoscience and Mineral Resources, Daejeon, 124, Gwahang-no, Yuseong-gu, Daejeon 34132, Korea; kkt@kigam.re.kr

[2] School of Earth System Science, Kyungpook National University, Daegu 41566, Korea; naress@knu.ac.kr

*   Correspondence: sungwon@kigam.re.kr; Tel.: +82-42-868-3501

Abstract: Cretaceous volcano-sedimentary basins and successions in the Korean Peninsula are located along NE-SW- and NNE-SSW-trending sinistral strike–slip fault systems. Soft-sediment deformation structures (SSDS) of lacustrine sedimentary strata occur in the Wido, Buan, and Haenam areas of the southwestern Korean Peninsula. In this study, systematic geological, geochronological, and geochemical investigations of the volcanic-sedimentary successions were conducted to constrain the origin and timing of SSDS-bearing lacustrine strata. The SSDS-bearing strata is conformably underlain and overlain by volcanic rocks, and it contains much volcaniclastic sediment and is interbedded with tuffs. The studied SSDSs were interpreted to have formed by ground shaking during syndepositional earthquakes. U-Pb zircon ages of volcanic and volcaniclastic rocks within the studied volcano-sedimentary successions were ca. 87–84 Ma, indicating that active volcanism was concurrent with lacustrine sedimentation. Geochemical characteristics indicate that these mostly rhyolitic rocks are similar to subduction-related calc-alkaline volcanic rocks from an active continental margin. This suggests that the SSDSs in the study area were formed by earthquakes related to proximal volcanic activity due to the oblique subduction of the Paleo-Pacific Plate during the Late Cretaceous.

1. Introduction

In continental arcs and adjacent areas, tectonomagmatic activities produce a variety of sedimentary basins commonly filled with volcanic and volcaniclastic rocks that form volcano-sedimentary successions [1–4]. Although the successions are unique rock records that unravel syndepositional tectonism and volcanism and their genetic relationships, the intrusion of magma along, or covering of volcanic rocks over, basin margins commonly make reconstruction of the tectonic activities difficult. During sedimentation of the successions, crustal deformation due to tectonic activity gives rise to moderate to strong earthquakes (Mw; moment magnitude > 5.0) [5]. The passage of seismic waves through near-surface, unconsolidated sediments can result in the development of soft-sediment deformation structures (SSDS) over a wide area (>10 km from the epicenter) as a result of liquefaction and/or fluidization due to elevated pore water pressure [6,7]. As a result of their wide occurrence, SSDSs have a high potential for preservation [8]. Thus, analysis of SSDSs is able to determine syndepositional tectonic activities, which can provide clues to unravel the genetic relationships between tectonic and magmatic activities in the continental arc and adjacent areas.

During the Cretaceous, volcano-sedimentary basins formed along sinistral strike–slip fault systems in the central to southwestern part of the Korean Peninsula (Figure 1) due to tectonomagmatic activities caused by oblique subduction of the Paleo-Pacific Plate [9–13].

Sedimentary successions within the basins were deposited in alluvial fan, fluviolacustrine, and lacustrine environments [14–16]. Vertical changes in the depositional environments and sedimentary characteristics (such as grain size and stacking patterns) have been interpreted as the result of syndepositional tectonic subsidence of the basins [14]. However, bounding faults of the basins are commonly obscured by volcanic intrusions or covered by volcanic rocks, preventing detailed analysis of the timing of tectonic activities. Recently, SSDSs within lacustrine strata of these basins have been interpreted to be the result of earthquakes, providing clues to unravel tectonic activities during sedimentation [12,17–19]. In this study, we present a systematic geological, geochronological, and geochemical investigation of the origin and timing of SSDS-bearing strata to constrain the origin and timing of tectonomagmatic activities in the Korean Peninsula and adjacent areas.
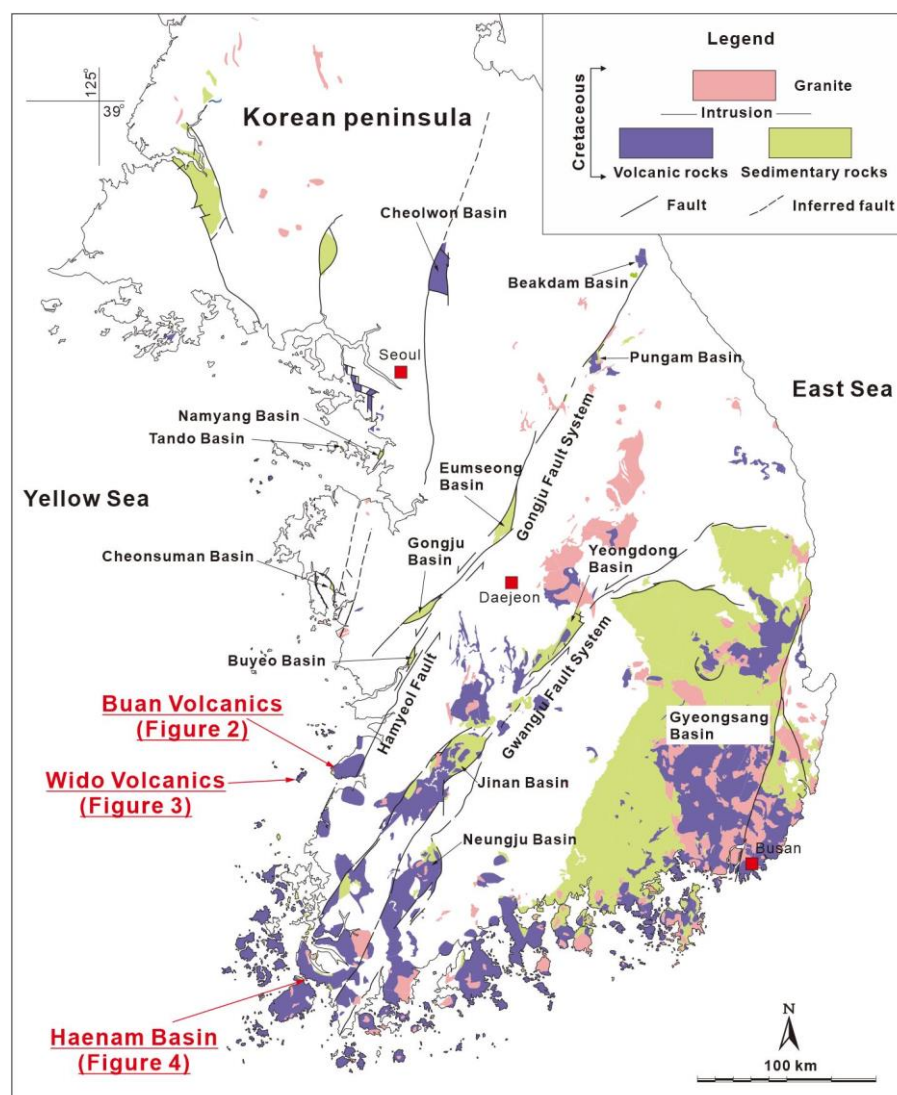
Figure 1. Map of the southern Korean Peninsula showing the distribution of Cretaceous sedimentary basins, and volcanic and igneous rocks along sinistral strike–slip fault systems (modified from [12]).

2. Geological Setting

During the Cretaceous, the Korean Peninsula was subjected to crustal deformation due to the oblique subduction of the Izanagi Plate beneath the Eurasian Plate [9,20–22]. The crustal deformation caused the formation of NE-SW and NNE-SSW-trending, sinistral strike–slip fault systems, such as the Gongju, Hamyeol, and Gwangju Fault systems, along with the development of back-arc basins in the southeastern part of the Korean Peninsula

(Figure 1). Along the fault systems, particularly in areas of step-over and releasing bends, small-scale, non-marine sedimentary basins formed and filled with fluviolacustrine sedimentary successions under arid to semi-arid climatic conditions [23]. Contemporaneously, continental arc volcanism produced large amounts of volcaniclastic sediment and volcanic rocks interbedded with sedimentary strata, forming volcano-sedimentary successions. Detailed observations of the volcano-sedimentary successions showed that the stacking patterns and spatial distribution of the volcanic-sedimentary lithofacies were the result of spatiotemporal variations in sediment supply related to explosive volcanism and accommodation space due to syndepositional tectonic activities, which has been interpreted to result from contemporaneous tectonomagmatic activities during the Cretaceous [14,15,24,25].

3. SSDS Bearing Volcano-Sedimentary Successions

To unravel the genetic relationships between SSDS-bearing strata and the circumstances behind SSDS formation and Cretaceous tectonomagmatism in the Korean Peninsula, this study focused on three SSDS-bearing, lacustrine volcano-sedimentary successions such as Beolgeumri, Gyeokpori, and Uhangri Formations [24,26,27]. These formations are underlain and overlain by or interbedded with volcanic and volcaniclastic rocks.

3.1. Beolgeumri Formation

The Beolgeumri Formation is a lithostratigraphic unit of the Wido Volcanics composed of conformably stacked volcanic, volcaniclastic, and sedimentary rocks. Koh et al. [28] classified the succession into four lithostratigraphic units from bottom to top: the Daeri Andesite, Mangryeongbong Tuff, Beolgeumri Formation, and Ttandallae Tuff (Figure 2A,B).
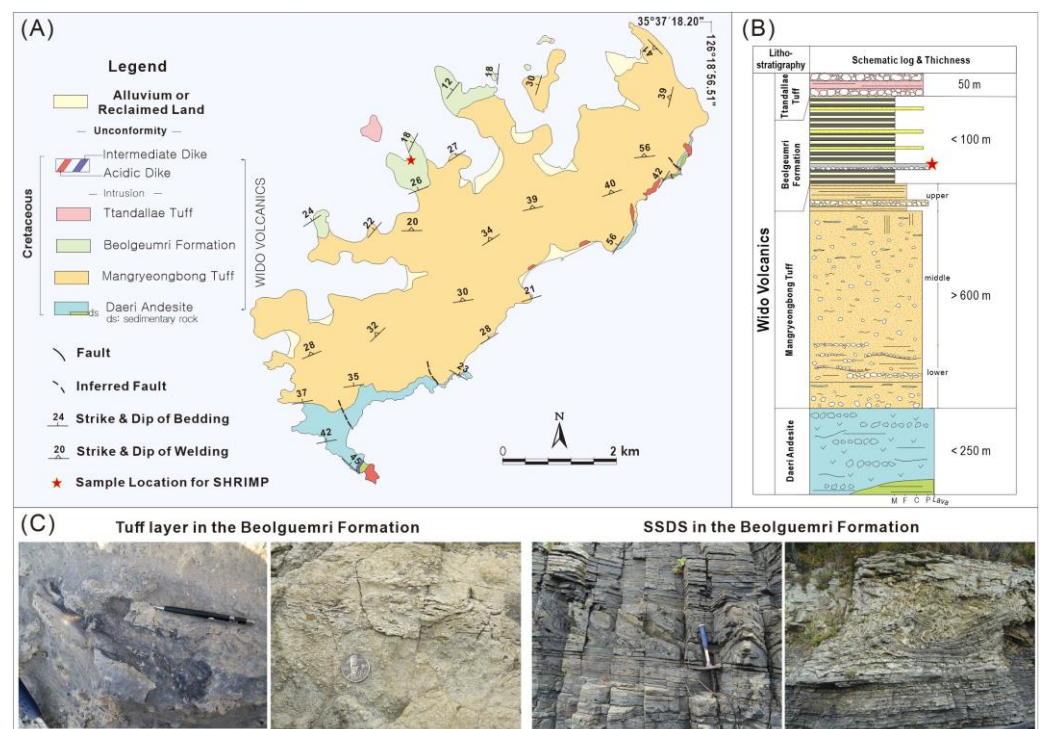
Figure 2. (**A**) Geological map of the Wido Volcanics (modified after [28]), (**B**) Schematic log of the volcano-sedimentary succession in the Wido Volcanics (modified after [12]), (**C**) Outcrop photographs of tuff layer and soft sediment deformation structures (SSDS) in the Beolgeumri Formation.

The Daeri Andesite is the lowermost lithostratigraphic unit of the volcanics and is composed of aphyric to porphyritic andesite underlain by dinosaur-egg bearing purple-colored mudstones [29,30]. Gihm et al. [25] interpreted that the Daeri Andesite was emplaced by subaerial lava flows in arid to semi-arid floodplain environments. The

overlying Mangryeongbong Tuff is about 900 m thick and consists mainly of rhyolitic volcaniclastic sediments formed by pyroclastic density currents. The Beolgeumri Formation between the Mangryeongbong and topmost Ttandallae Tuffs is composed of lacustrine mudstones and sandstones, chert, and a bed of lapilli tuff that were deposited in a lacustrine environment at the terminal part of a regional strike–slip fault system on the southwestern Korean Peninsula [12,25]. Ko et al. [12] reported that the Beolgeumri Formation contains various types of SSDS that are characterized by their wide extent (>4 km), lateral continuity (>200 m), and vertical repetition. The SSDSs are underlain and overlain by undeformed laminated mudstones (Figure 2C). These indicate that the SSDSs were formed mainly by liquefaction and/or fluidization triggered by ground shaking during earthquakes [12]. The topmost Ttandallae Tuff is estimated to be about 40 m thick and is composed of tuff breccias and lapilli tuff deposited by pyroclastic density currents [12].

The weighted mean of $^{206}Pb/^{238}U$ zircon ages from the Mangryeongbong and the Ttandallae tuffs yielded 86.63 ± 0.83 Ma (n = 14, 2σ, MSWD = 2.0) and 87.25 ± 0.36 Ma (n = 13, 2 σ, MSWD = 1.09), respectively [12].

3.2. Gyeokpori Formation

The Gyeokpori Formation belongs to the Buan Volcanics and is classified into numerous stratigraphic units of volcaniclastic and volcanic rocks (Cheonmasan Tuff, Udongje Tuff, Seokpo Tuff, Gyeokpori Formation, Gomso Rhyolite, Yujeongge Tuff, Byeonsan Tuff, and Samyebong Rhyolite in ascending order [28] (Figure 3A,B). The Gyeokpori Formation between the Seokpo Tuff and Gomso rhyolite is composed of conglomerates, gravelly sandstones, mudstones, and beds of volcaniclastic deposits. The Gyeokpori Formation is interpreted to have been deposited in lacustrine environments with a small-scale, steeply sloped delta system at the lake margin [24]. A number of SSDS are observed in sandstone and mudstone lake floor deposits (not on the steeply inclined delta). Ko et al. [18] reported that slump structures in the Gyeokpori Formation are about 2 m thick, laterally continuous (>200 m), and repeated vertically. These structures are underlain and overlain by undeformed laminated black mudstones consisting of folds and syn-depositional (thrust and normal) faults (Figure 3C). In addition, Byun et al. [31] reported chaotically deformed layers in the Gyeokpori Formation that were triggered by seismic shocks.
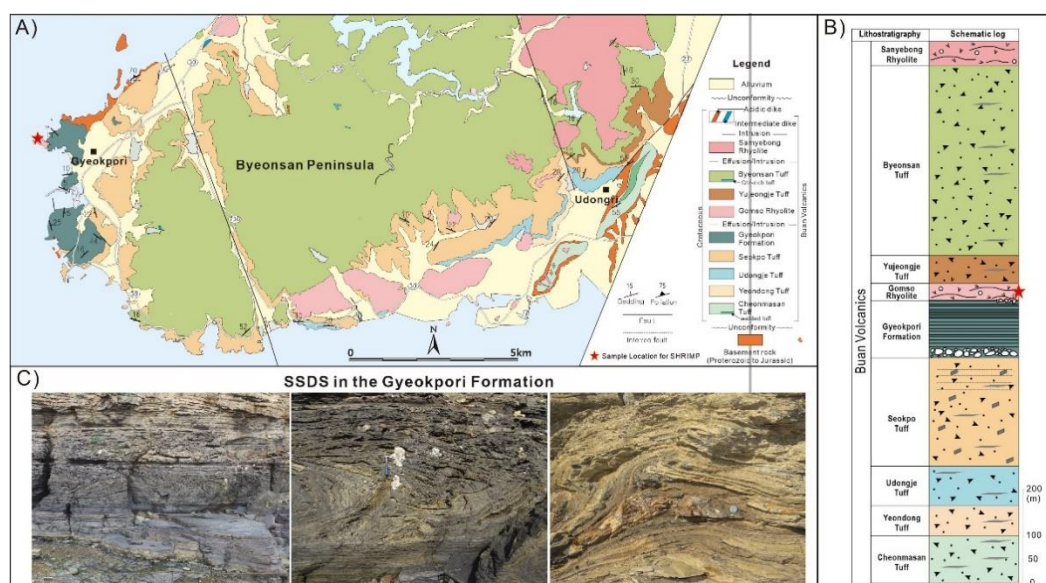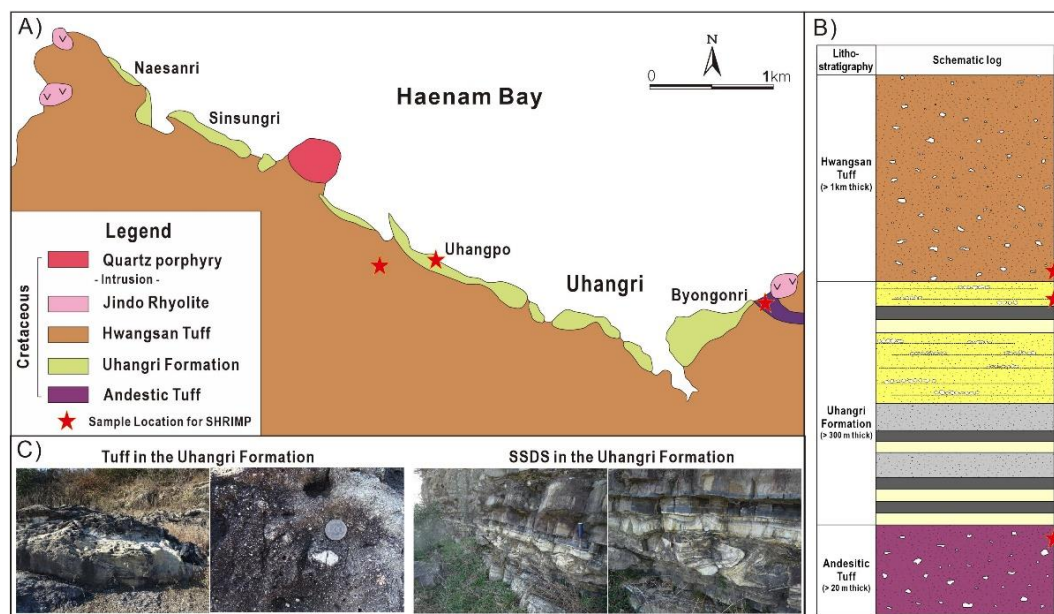

Figure 3. (**A**) Geological map of the Buan Volcanics (modified after [28]), (**B**) Schematic log of the volcano-sedimentary succession in the Buan Volcanics (modified after [13]), (**C**) Outcrop photographs of soft sediment deformation structures (SSDS) in the Gyeokpori Formation.

The weighted mean of $^{206}Pb/^{238}U$ zircon ages from conformably underlying (Seokpo Tuff) and unconformably overlying (Yujeongge Tuff) strata yielded 87.30 ± 0.99 Ma (*n* = 15, 2σ, MSWD = 2.0) and 86.66 ± 0.93 Ma (*n* = 20, 2 σ, MSWD = 2.8), respectively [13].

3.3. Haenam Basin

The Late Cretaceous Uhangri Formation is a volcano-sedimentary succession deposited in the Haenam Basin in the southwestern part of the Korean Peninsula (Figure 1). The Uhangri Formation is underlain by andesitic tuff and overlain by the Hwangsan Tuff and Jindo Rhyolite (Figure 4A,B). The Uhangri Formation mainly consists of conglomerate, sandstone, laminated shale, and cherty mudstone with interlayered volcaniclastic deposits, deposited in alluvial, lacustrine delta, and lacustrine environments [26,32,33]. A number of fold structures and convolute laminations are found in specific layers of the lacustrine sandstones and mudstones. These intervals are underlain and overlain by undeformed laminated to homogeneous mudstones (Figure 4C). This indicates that these SSDSs were formed by the deformation of unconsolidated sediments via liquefaction and associated fluidization triggered by earthquakes. Chough and Chun [34] also reported intrastratal flows and associated rip-down structures in deltaic sediments. They interpreted these structures to have been formed by syndepositional earthquakes.

Figure 4. (**A**) Geological map of the Haenam Basin (modified after [34]), (**B**) Schematic log of the volcano-sedimentary succession in the Haenam Basin (modified after [35]), (**C**) Outcrop photographs of tuff layer and soft sediment deformation structures (SSDS) in the Uhangri Formation.

4. Analytical Methods

Representative volcanic and sedimentary samples associated with soft-sediment deformation structures were collected from the volcanic and volcaniclastic rocks situated within, underlying, or overlying Cretaceous lacustrine sediments. Zircon grains were extracted from crushed rocks by heavy liquid and magnetic separation, followed by handpicking under a binocular microscope. Observation of the internal structure of the zircon grains before analysis was carried out using back-scattered electron and cathodoluminescence (CL) imaging, which were performed using the JEOL6610LV scanning electron microscope at the Korea Basic Science Institute.

For SHRIMP U-Pb dating, zircon grains were mounted in epoxy resin disks, along with chips of the FC1 (Duluth gabbro of 1099 Ma [36]) and SL13 (Sri Lankan gem zircon, U = 238 ppm [37]) reference zircons. U-Th-Pb isotopic composition analysis followed the

protocols of Williams [38] and Kim et al. [11]. The wavelength and current of the primary ion beam used in the analysis were $\approx$30 µm and $\approx$3 nA, respectively. For the calculation of U and Th contents in zircon, SL13 was used as the reference, while the $^{206}Pb/^{238}U$ ratio was calibrated using the FC1 zircon standard ($^{206}Pb/^{238}U$ = 0.1859 [36]). Common Pb contributions were corrected using the measured ^{204}Pb and the model common Pb composition suggested by Stacey and Kramers [39]. The isotopic ratio of Pb-Th-U in the analyzed zircon and the weighted mean age were calculated using SQUID 2.50 and Isoplot 3.71 [40,41]. Each of the analysis points marked on the Tera–Wasserburg diagram used values that were not corrected for $^{204}Pb_c$ and had an error range of 2σ. The suggested mean zircon ages were ^{207}Pb corrected $^{206}Pb/^{238}U$ ages, and uncertainties were calculated at a confidence level of 95 %. The zircon U-Pb age data are summarized in Table S1.

Fourteen volcanic rocks were analyzed for whole-rock major and trace element abundances, and rare earth element (REE) abundances using inductively coupled plasma atomic emission spectrometry (Thermo Jarrel-Ash ENVIRO II) and ICP mass spectrometry (Perkin–Elmer Optima 3000) at Activation Laboratories, Ltd.(Ancaster, ON, Canada). Analytical uncertainties ranged from 1% to 3%.

5. Results

5.1. Zircon U-Pb Dating

5.1.1. Tuff Bed in the Beolgeumri Formation

Zircon grains from a tuff (BT-1) in the Beolgeumri Formation were fine- to medium-grained (20–200 µm diameter) euhedral prismatic grains (Figure 5A). The aspect ratios ranged from 1 to 3. CL imaging showed that the grains had oscillatory zoning, showing well-developed sector zoned areas. The 15 analyses by SHRIMP U-Pb dating gave a weighted mean $^{206}Pb/^{238}U$ age of 87.1 ± 1.0 Ma (n = 15, 2σ, MSWD = 1.8) (Figure 6A).
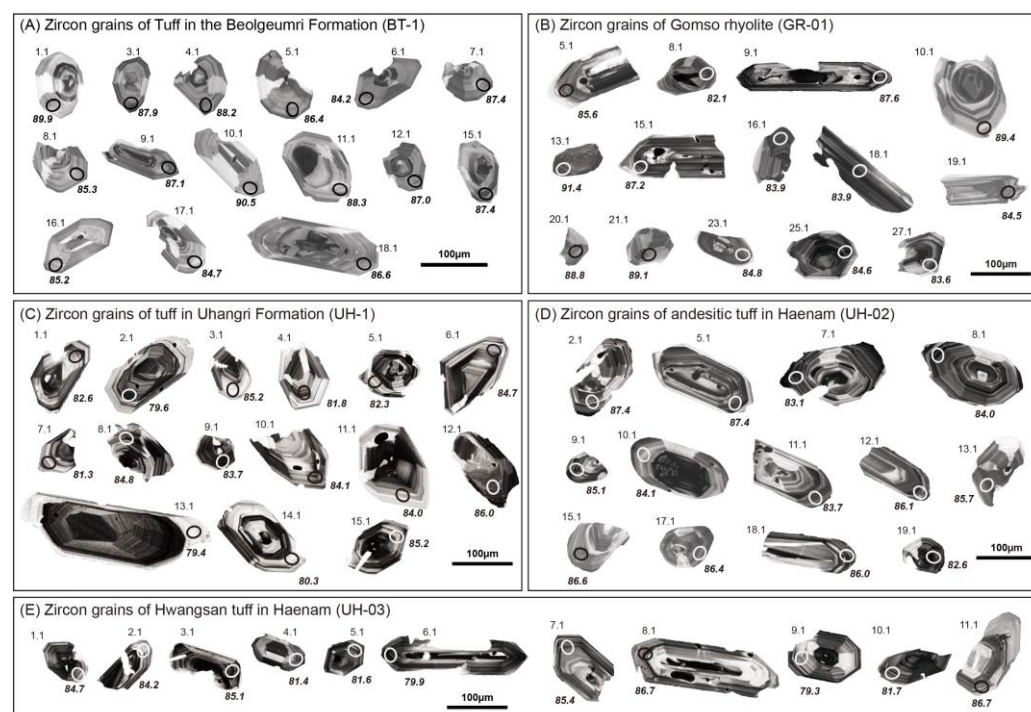
Figure 5. Cathodoluminescence (CL) images of zircon grains from (**A**) the tuff in the Beolgeumri Formation, (**B**) the Gomso Rhyolite, (**C**) the tuff in the Uhangri Formation, (**D**) the andesitic tuff, and (**E**) the Hwangsan Tuff. Analyzed points and ages (bold italics) are shown.
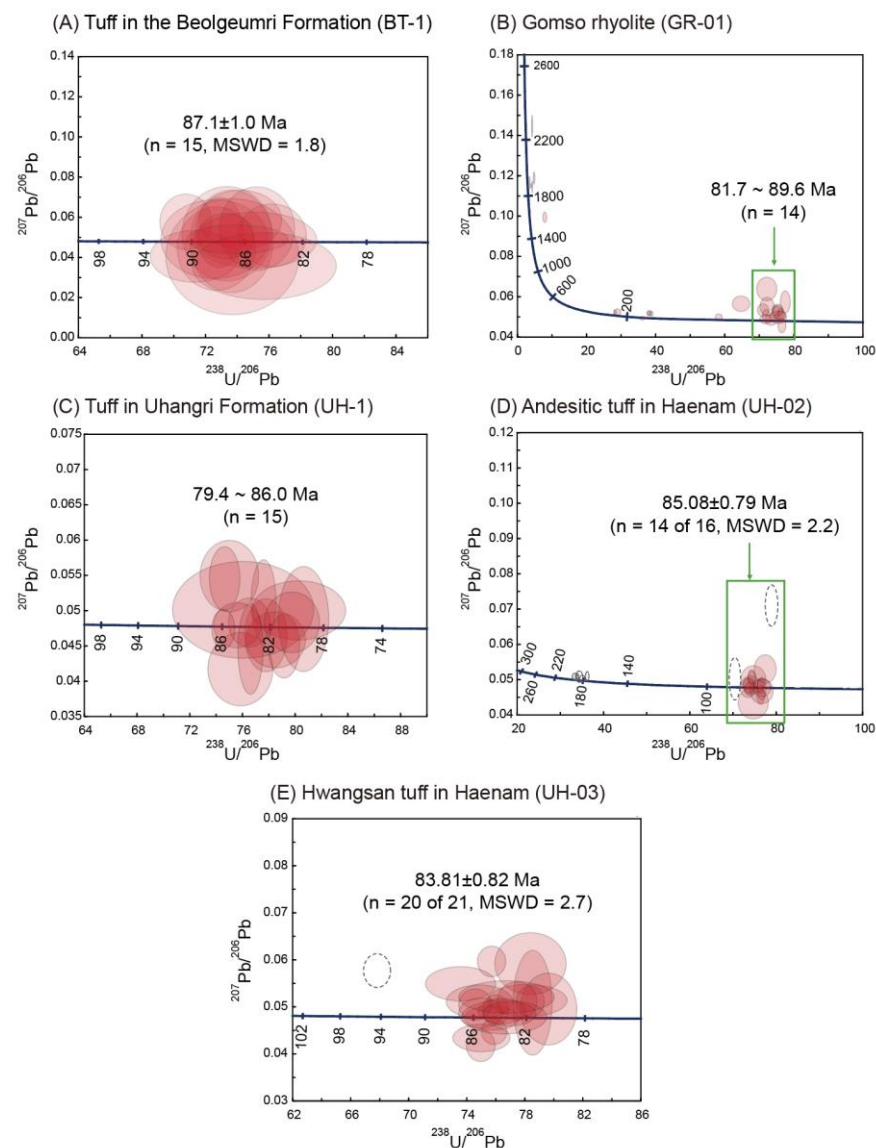
Figure 6. Concordia plots of the SHRIMP U-Pb isotopic analyses of zircons from (**A**) the tuff in the Beolgeumri Formation, (**B**) the Gomso Rhyolite, (**C**) the tuff in the Uhangri Formation, (**D**) the andesitic tuff, and (**E**) the Hwangsan tuff with analyzed points and ages. Gray dotted ellipsoids were excluded from weighted mean calculations.

5.1.2. Gomso Rhyolite in the Buan Volcano-Sedimentary Succession

Zircon grains from the Gomso Rhyolite (GR-1) in the Buan volcano-sedimentary succession of the Buan area were fine- to coarse-grained (25–250 μm diameter) and had aspect ratios ranging from 1 to 4. The CL images showed that about 40% of zircon grains were euhedral to subhedral and have clear oscillatory zoning of the whole grain. Some zircon grains are composites, consisting of inherited cores surrounded by very thin, bright CL, and magmatic overgrowths. The cores are characterized by sector and oscillatory zoning (Figure 5B). The combined $^{206}Pb/^{238}U$ and $^{207}Pb/^{206}Pb$ apparent ages of many of the inherited zircons by SHRIMP U-Pb dating have high discordance due to Pb loss or contamination, and they range from Middle Paleoproterozoic to early Late Cretaceous, as follows: 1912 Ma, 1875–1860 Ma (*n* = 4), 226 Ma, 168–165 Ma, 110 Ma, and 97 Ma. Analyses of the youngest euhedrally zoned grains show variable $^{206}Pb/^{238}U$ ages from 89.6 Ma to 81.7 Ma (*n* = 14; Figure 6B). The Seokpo Tuff in the Buan Volcanics is older than the Gomso Rhyolite; it extruded at 88.7 ± 2.0 Ma (*n* = 10, MSWD = 2.2) [28].

5.1.3. Volcanic Rocks in the Haenam Basin

Zircon grains from a tuff (UH-1) in the Uhangri Formation were fine- to coarse-grained (20–300 μm diameter) and had euhedral to subhedral shapes. The aspect ratios ranged from 1 to 3. CL images showed that most zircon grains contained prismatic oscillatory and sector zoning of the whole grain (Figure 5C). SHRIMP U-Pb dating of euhedrally-zoned grains showed slightly variable ages from 89.0 Ma to 79.4 Ma (Figure 6C).

Zircon grains from an andesitic tuff (UH-2) that underlies the Uhangri Formation were predominantly small to large (20–200 μm diameter) euhedral prismatic grains with aspect ratios ranging from 1 to 5 (Figure 5D). However, some grains had rounded crystal terminations. CL imaging showed that the grains had well-developed euhedral oscillatory zoning with sector-zoned areas. For SHRIMP U-Pb dating, the analyzed grains showed two age clusters: Early Jurassic (192–177 Ma) and Late Cretaceous (91–79 Ma). The younger $^{206}Pb/^{238}U$ apparent ages of the euhedral zoned grains show a relatively tight cluster at about 87.1–82.2 Ma, excluding statistical outliers (90.8 Ma and 78.8 Ma). The age results yielded a weighted mean $^{206}Pb/^{238}U$ age of 85.08 ± 0.79 Ma (n = 14 of 16, MSWD = 2.2; Figure 6D).

Zircon grains (15–350 μm diameter) from the Hwangsan Tuff (UH-3) were subhedral to euhedral and preserved euhedral oscillatory zoning (Figure 5E). SHRIMP U-Pb analyses (n = 21) yielded an age range between 86.2 and 81.3 Ma, with one exception (93.3 Ma). Although they gave a weighted mean $^{206}Pb/^{238}U$ age of 83.81 ± 0.82 Ma (n = 20 of 21, MSWD = 2.7), the age $^{206}Pb/^{238}U$ apparent ages were slightly variable (Figure 6E).

5.2. Geochemistry

Volcanic samples from the Wido, Buan, and Haenam volcano-sedimentary successions were analyzed to determine the geochemical signatures (Table S2).

On the SiO_2 versus $Na_2O + K_2O$ diagram (Figure 7), the Wido, Buan, and Haenam volcanic and volcanoclastic rock samples mostly plot in the rhyolite field. The samples display the following variations in major element contents: SiO_2 (67.25–75.60 wt %), Al_2O_3 (12.90–16.52 wt %), TiO_2 (0.10–0.36 wt %), Fe_2O_3* (1.33–2.91 wt %), MgO (0.17–1.01 wt %), CaO (0.17–2.12 wt %), Na_2O (1.43–5.95 wt %), K_2O (2.11–6.08 wt %), and P_2O_5 (0.01–0.11 wt %) (Figure 8).
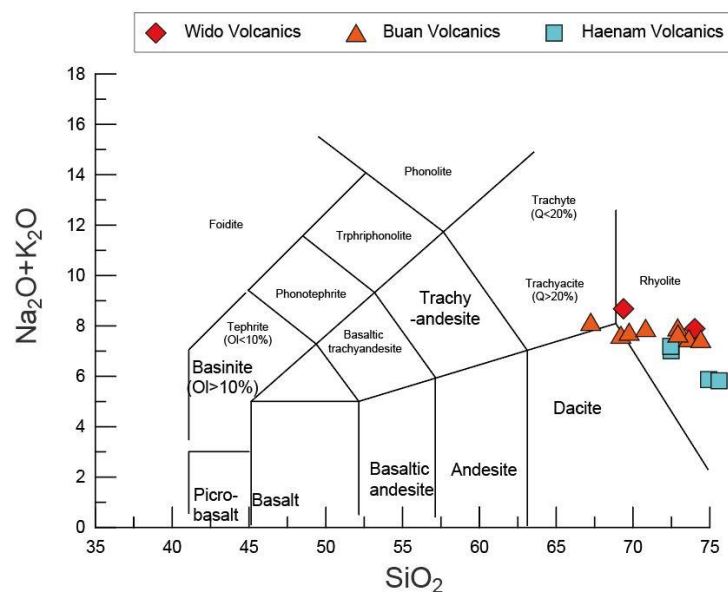
Figure 7. Diagrams of SiO_2 wt % versus $Na_2O + K_2O$ wt % for the Cretaceous volcanic rocks from the southwestern Korean Peninsula.
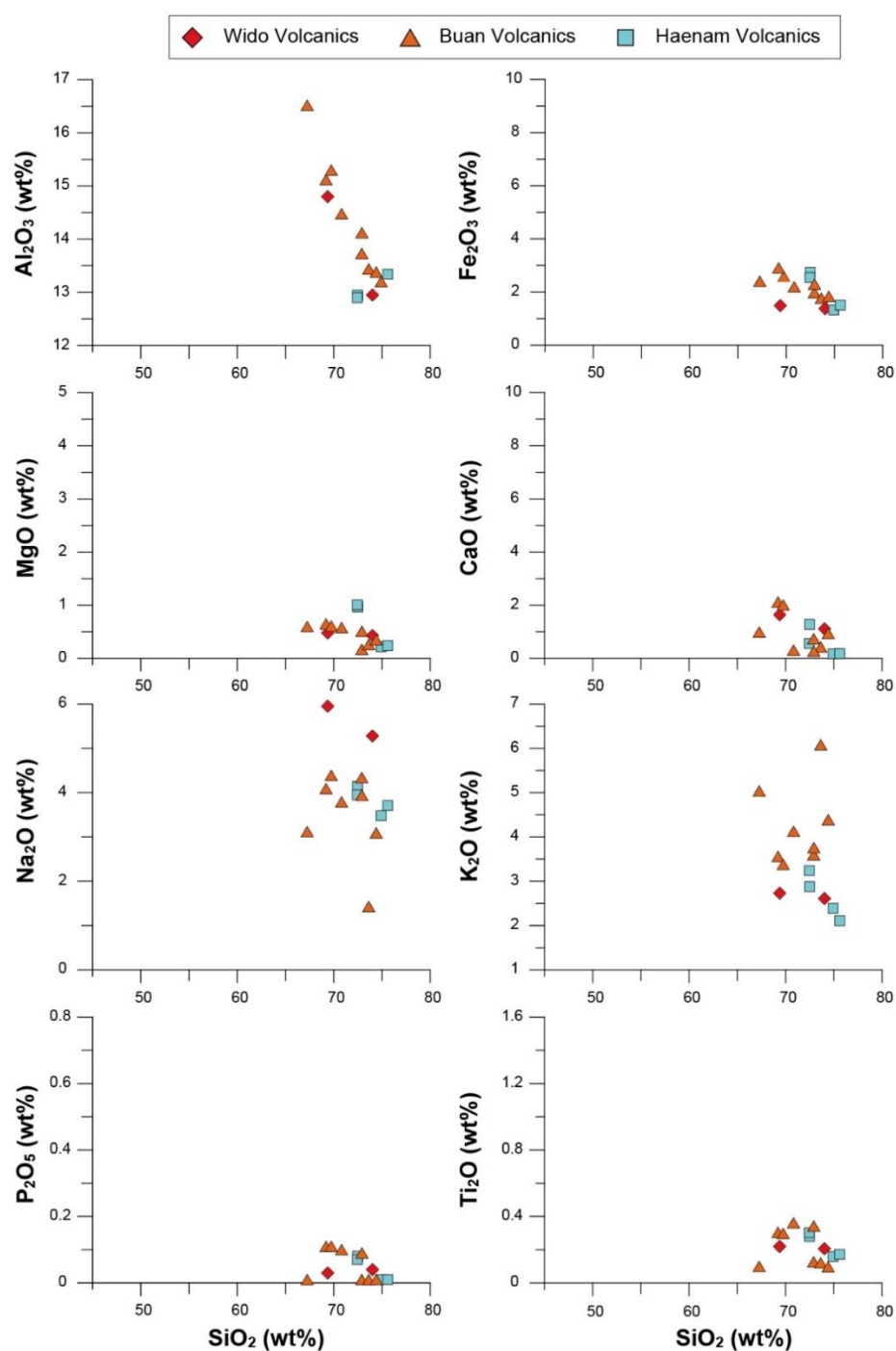
Figure 8. Plots of major elements vs. SiO$_2$ for the Cretaceous volcanic rocks from the southwestern Korean Peninsula.

The Wido, Buan, and Haenam volcanic and volcaniclastic rock samples display LREE depletion with strongly to weakly negative Eu anomalies (Eu/Eu* = 0.33−0.96) in the chondrite-normalized REE diagrams (Figure 9A,C,E). On the primitive mantle normalized diagrams (Figure 9B,D,F), the samples display large ion lithophile element enrichment with Ta–Nb troughs and depletion in P and Ti, indicating arc-related volcanism.
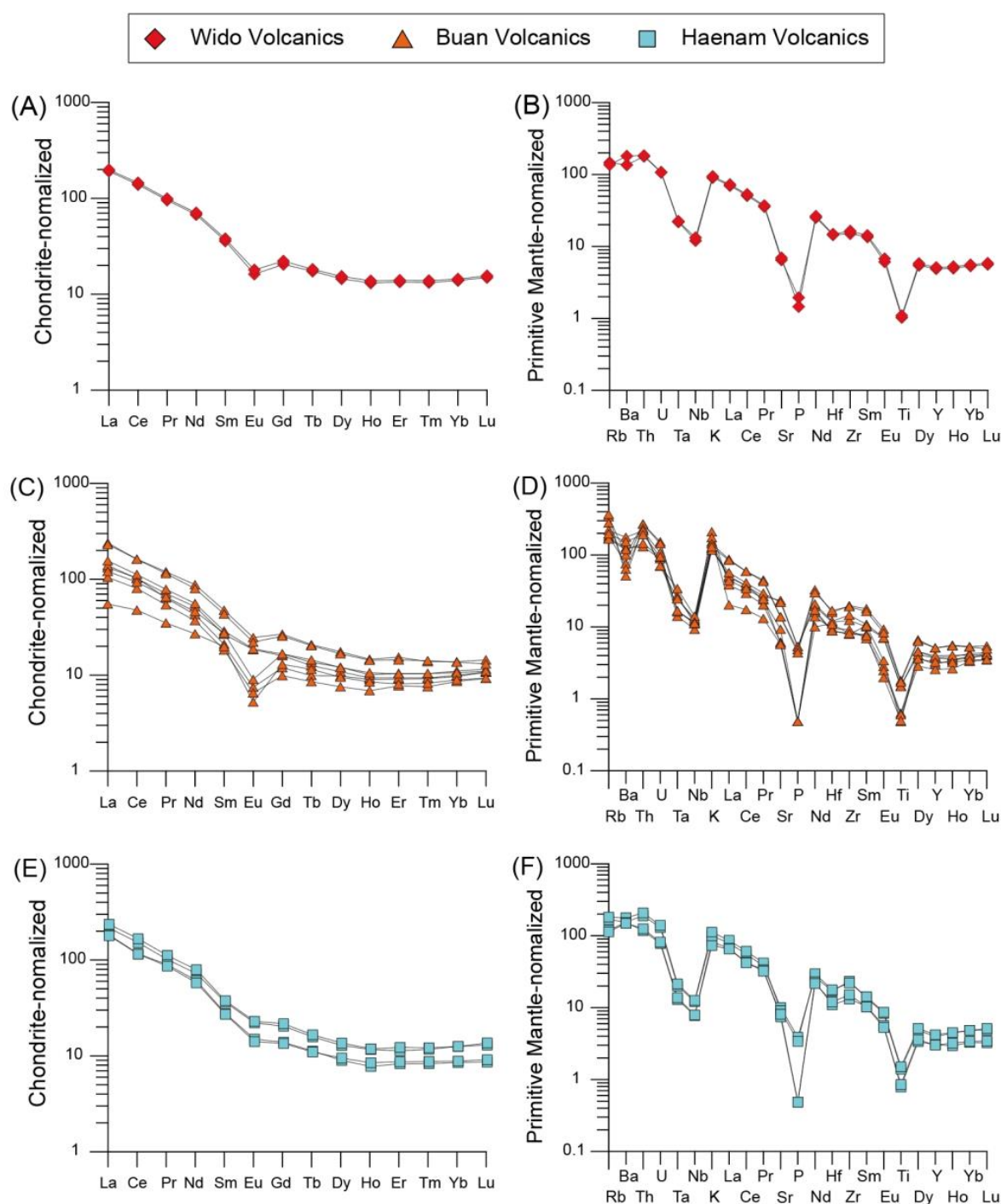
Figure 9. Chondrite-normalized rare earth element and primitive mantle-normalized trace element for the Cretaceous volcanic rocks from the southwestern Korean Peninsula.

6. Discussion

The SSDS-bearing strata of the Beolgeumri, Gyeokpori, and Uhangri Formations were deposited in lacustrine environments during 87–84 Ma. These formations are underlain and overlain by tuffs formed by explosive volcanic eruptions, suggesting the development of a lake during the interval between the depositions of the thick volcaniclastic successions. Volcaniclastic sediments (Gyeokpori Formation) and tuff beds (Beolgeumri and Uhangri Formations) also indicate syndepositional volcanic influences on sedimentation in the lacustrine environments.

Modern and Quaternary data show that large amounts of unconsolidated volcaniclastic sediments are dispersed on volcanoes and surrounding areas by pyroclastic density currents and fall out from the eruption column during and immediately after explosive volcanic eruptions [42]. The fine-grained and poorly sorted nature of volcaniclastic sediments prevents infiltration of rainwater into the substrate. This causes an increase in surface runoff, resulting in frequent flooding (e.g., lahar) after explosive volcanic eruptions [43]. The flood water erodes and carries large amounts of unconsolidated sediment toward lowlands. Therefore, the rates of sediment supply are increased dramatically—enough to reduce topographic relief by the filling of lowlands via sedimentation [44,45]. Despite high rates of sediment supply after the explosive eruptions, the SSDS-bearing, Beolgeumri, Gyeokpori, and Uhangri Formations accumulated in the lake during and after the eruptions. This indicates that the preservation of lacustrine environments during sedimentation, and rates of accommodation space creation exceeded or at least compensated for the sedimentation rates with the forceful input of sediment.

The creation of accommodation space could be attributed to a wet climate that caused an increase in the amount of water flowing into the lake. However, Late Cretaceous sedimentary successions in the Korean Peninsula commonly contain evaporites, calcrete nodules, and raindrop prints, indicating arid to semi-arid climatic conditions [23,46]. Thus, the creation of the accommodation space was interpreted to have resulted from tectonic subsidence, which lowered lake floors. Tectonic subsidence commonly involves moderate and strong earthquakes [5]. Previous studies targeting the SSDS-bearing strata of the Beolgeumri, Gyeokpori, and Uhangri Formations suggest that SSDSs were formed by ground shaking during syndepositional earthquakes [12,18,19,34]. During field observations, we found that all SSDSs are underlain and overlain by undeformed laminated or homogeneous mudstones, suggesting that these SSDSs were not related to depositional events such as slumps. In addition, possible triggering mechanisms for SSDSs, such as rapid sedimentation and passage of large waves (> 10 m in wave height), cannot be applied to lacustrine environments [6,7]. Thus, the development and preservation of the lacustrine environments in which SSDS-bearing strata were deposited were likely due to syndepositional tectonic subsidence, and concomitant earthquakes caused the deformation of the sediments, forming the SSDSs.

The geochemical and geochronological data also support this interpretation. The trace element and REE geochemical characteristics of volcanic rocks are similar to those of subduction-related calc-alkaline volcanic rocks from active continental margins. In the classification of Pearce et al. [47], the Wido, Buan, and Haenam rhyolitic volcanic and volcaniclastic samples occur in the volcanic arc granitoid field (Figure 10). During the late Cretaceous, a continental volcanic arc formed as a consequence of the oblique subduction of the Paleo-Pacific Plate. The arc volcanism produced large amounts of volcaniclastic sediment. Contemporaneously, oblique subduction of the Izanagi Plate underneath the Eurasian Plate caused sinistral strike–slip crustal deformation. The sedimentary basins of strike–slip fault systems are characterized by rapid subsidence compared to extensional basins [48]. Geochronological data from numerous SHRIMP and IDTIMS studies [10–13,28,49–51] of the Cretaceous volcanic rocks can be divided into two age groups in the southern Korean Peninsula: (1) Early Cretaceous (115–96 Ma) volcanism related to the major sedimentation in the Gyeongsang Basin, and (2) Late Cretaceous (91–77 Ma) regional volcanism and minor sedimentation in the southern Korean Peninsula, with maximal activity at 87–85 Ma (Figure 11). Thus, from 87 to 84 Ma, the southwestern part of the Korean Peninsula was affected by vigorous tectonomagmatic activities, not only producing large amounts of volcaniclastic sediment but also creating sufficient accommodation space due to tectonic subsidence, as reflected by the SSDSs in lacustrine sediments of the volcano-sedimentary successions.
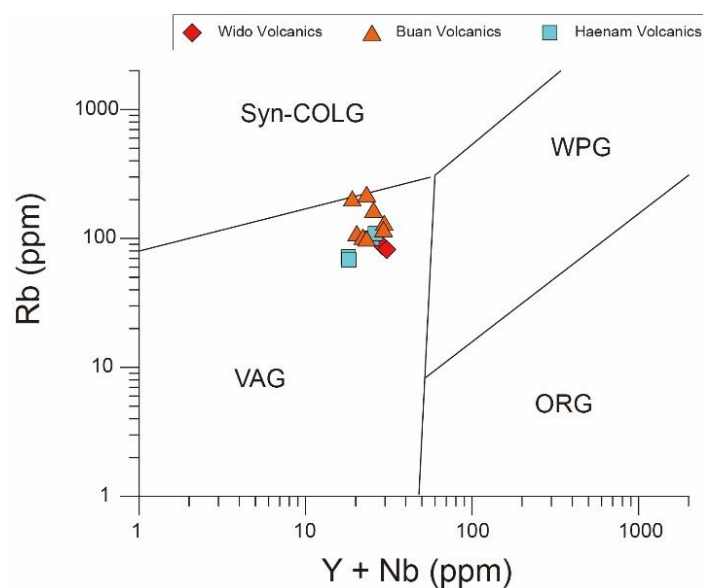
Figure 10. Rb/(Y + Nb) tectonic discrimination diagrams [47]. VAG, volcanic arc granitoids; ORG, ocean ridge granitoids; WPG, within-plate granitoids; syn-COLG and post-COLG, syn- and post-collision granitoids; late and post-COLG, late- and post-collision granitoids.
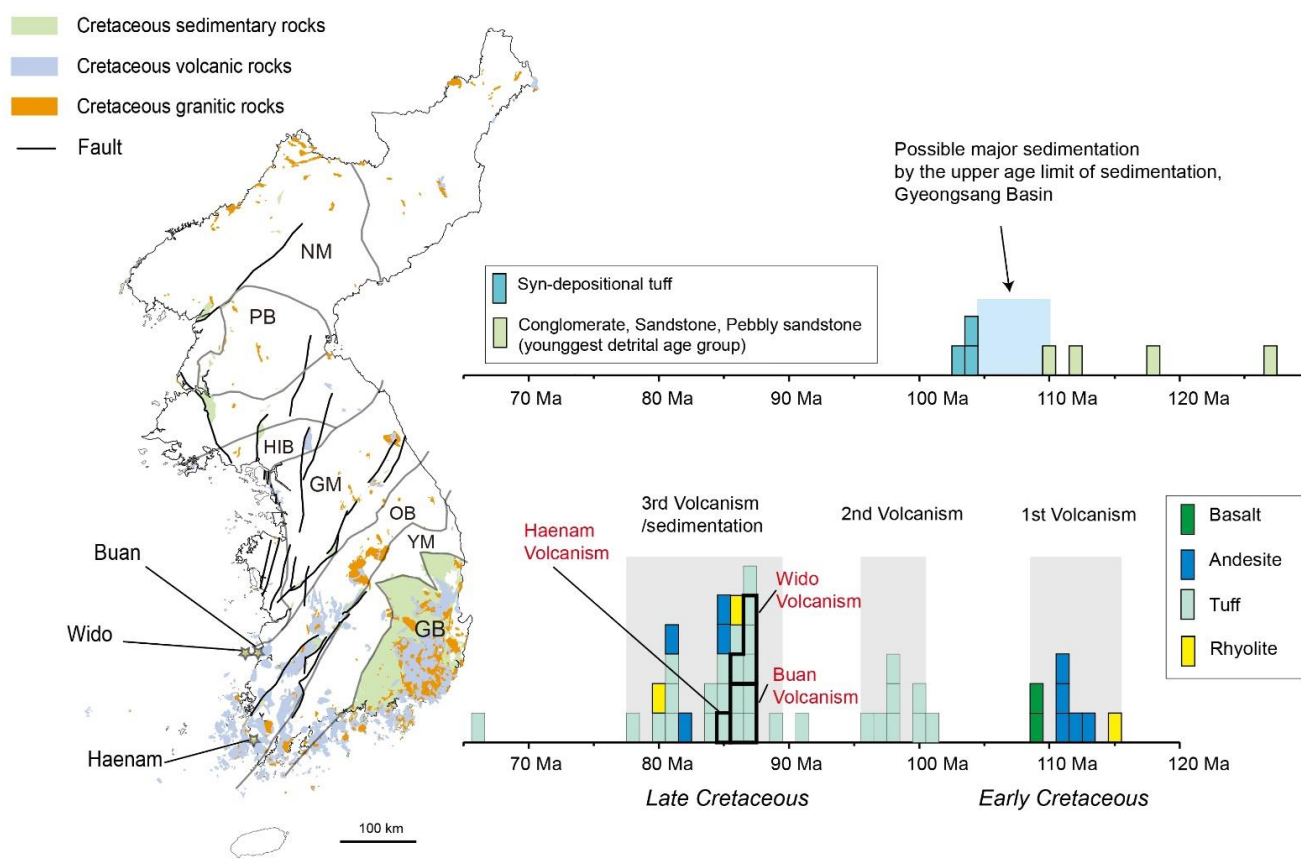
Figure 11. Frequency distribution diagrams of SHRIMP and IDTIMS zircon U-Pb ages for the Cretaceous volcanic and sedimentary rocks by the rock occurrence patterns throughout the Korean Peninsula.

7. Conclusions

(1) Cretaceous volcano-sedimentary successions in the Wido, Buan, and Haenam areas of the central to southwestern part of the Korean Peninsula are distributed along the sinistral strike–slip fault systems.

(2) SSDS-bearing lacustrine strata of the Beolgeumri, Gyeokpori, and Uhangri Formations were deposited during a period of syndepositional active volcanism between 87 and 84 Ma.

(3) The volcanic and volcaniclastic rocks in this study have the geochemical characteristics of subduction-related calc-alkaline volcanic rocks from active continental margins.

(4) The SSDS-bearing strata were interpreted to have been deposited as a result of syndepositional tectonic subsidence and deformed by syndepositional earthquakes in the southwestern Korean Peninsula during the Late Cretaceous.

Supplementary Materials: The following are available online at https://www.mdpi.com/article/10.3390/min11050520/s1, Table S1: SHRIMP U-Pb zircon data of the Late Cretaceous volcano-sedimentary successions, South Korea. Table S2: Major and trace element analyses of the Cretaceous volcanic rocks in the Wido, Buan and Haenam areas in the SW Korean Peninsula.

Author Contributions: Conceptualization, data acquisition, writing-original draft preparation, visualization, K.K.; writing—original draft, data acquisition, visualization, S.K.; data acquisition, writing—review and editing, Y.G. All authors have read and agreed to the published version of the manuscript.

Institutional Review Board Statement: Not applicable.

Informed Consent Statement: Not applicable.

Data Availability Statement: Not applicable.

Conflicts of Interest: The authors declare no conflict of interest.

References

1. Busby, C.J. Extensional and Transtensional Continental Arc Basins: Case Studies From the Southwestern United States. In *Tectonics of Sedimentary Basins: Recent Adv.*; Busby, C.J., Azor, A., Eds.; Blackwell Publishing: Hoboken, NJ, USA, 2012; pp. 382–404.
2. Acocella, V. Structural Control on Magmatism Along Divergent and Convergent Plate Boundaries: Overview, Model, Problems. *Earth Sci. Rev.* **2014**, *136*, 226–288. [CrossRef]
3. D'Elia, L.; Martí, J.; Muravchik, M.; Bilmes, A.; Franzese, J.R. Impact of Volcanism on the Sedimentary Record of the Neuquén Rift Basin, Argentina: Towards a Cause and Effect Model. *Basin Res.* **2018**, *30*, 311–335. [CrossRef]
4. Espinoza, M.; Montecino, D.; Oliveros, V.; Astudillo, N.; Vásquez, P.; Reyes, R.; Celis, C.; González, R.; Contreras, J.; Creixell, C.; et al. The Synrift Phase of the Early Domeyko Basin (Triassic, Northern Chile): Sedimentary, Volcanic and Tectonic Interplay in the Evolution of an Ancient Subduction-Related Rift Basin. *Basin Res.* **2019**, *31*, 4–32. [CrossRef]
5. Dorsey, R.J.; Umhoefer, P.J.; Falk, P.D. Earthquake Clustering inferred From Pliocene Gilbert-Type Fan Deltas in the Loreto Basin, Baja California Sur, Mexico. *Geology* **1997**, *25*, 679–682. [CrossRef]
6. Owen, G.; Moretti, M. Identifying Triggers for Liquefaction-Induced Soft-Sediment Deformation in Sands. *Sediment. Geol.* **2011**, *235*, 141–147. [CrossRef]
7. Owen, G.; Moretti, M.; Alfaro, P. Recognising Triggers for Soft-Sediment Deformation: Current Understanding and Future Directions. *Sediment. Geol.* **2011**, *235*, 133–140. [CrossRef]
8. Gihm, Y.S.; Kim, S.W.; Ko, K.; Choi, J.-H.; Bae, H.; Hong, P.S.; Lee, Y.; Lee, H.; Jin, K.; Choi, S.-J.; et al. Paleoseismological implications of liquefaction-induced structures caused by the 2017 Pohang Earthquake. *Geosci. J.* **2018**, *22*, 871–880. [CrossRef]
9. Chough, S.K.; Sohn, Y.K. Tectonic and Sedimentary Evolution of a Cretaceous Continental Arc–Backarc System in the Korean Peninsula: New View. *Earth Sci. Rev.* **2010**, *101*, 225–249. [CrossRef]

10. Kim, S.W.; Kwon, S.; Ryu, I.-C.; Jeong, Y.-J.; Choi, S.J.; Kee, W.-S.; Yi, K.; Lee, Y.S.; Kim, B.C.; Park, D.W. Characteristics of the Early Cretaceous Igneous Activity in the Korean Peninsula and Tectonic Implications. *J. Geol.* **2012**, *120*, 625–646. [CrossRef]

11. Kim, S.W.; Kwon, S.; Park, S.-I.; Lee, C.; Cho, D.-L.; Lee, H.J.; Ko, K.; Kim, S.J. SHRIMP U-Pb Dating and Geochemistry of the Cretaceous Plutonic Rocks in the Korean Peninsula: A New Tectonic Model of the Cretaceous Korean Peninsula. *Lithos* **2016**, *262*, 88–106. [CrossRef]

12. Ko, K.; Kim, S.W.; Lee, H.-J.; Hwang, I.G.; Kim, B.C.; Kee, W.-S.; Kim, Y.-S.; Gihm, Y.S. Soft Sediment Deformation Structures in a Lacustrine Sedimentary Succession Induced by Volcano-Tectonic Activities: An Example From the Cretaceous Beolgeumri Formation, Wido Volcanics, Korea. *Sediment. Geol.* **2017**, *358*, 197–209. [CrossRef]

13. Kwon, C.W.; Ko, K.; Gihm, Y.S.; Koh, H.J.; Kim, H. Late Cretaceous Volcanic Arc System in Southwest Korea: Distribution, Lithology, Age, and Tectonic Implications. *Cret. Res.* **2017**, *75*, 125–140. [CrossRef]

14. Ryang, W.H.; Chough, S.K. Sequential Development of Alluvial/Lacustrine System; Southeastern Eumsung Basin (Cretaceous), Korea. *J. Sediment. Res.* **1997**, *67*, 274–285.

15. Lee, S.H.; Chough, S.K. Progressive Changes in Sedimentary Facies and Stratal Patterns Along the Strike-Slip Margin, North-eastern Jinan Basin (Cretaceous), Southwest Korea: Implications for Differential Subsidence. *Sediment. Geol.* **1999**, *123*, 81–102. [CrossRef]

16. Kim, S.B.; Kim, Y.-G.; Jo, H.R.; Jeong, K.S.; Chough, S.K. Depositional Facies, Architecture and Environments of the Sihwa Formation (Lower Cretaceous), Mid-West Korea With Special Reference to Dinosaur Eggs. *Cret. Res.* **2009**, *30*, 100–126. [CrossRef]

17. Kang, H.C.; Paik, I.S.; Lee, H.I.; Lee, J.E.; Chun, J.H. Soft-Sediment Deformation Structures in Cretaceous Non-Marine Deposits of Southeastern Gyeongsang Basin, Korea: Occurrences and Origin. *Isl. Arc* **2010**, *19*, 628–646. [CrossRef]

18. Ko, K.; Park, S.; Kwon, C.W. Soft-Sediment Deformation Structures in the Cretaceous Gyeokpori Formation of the Buan Area, Korea: Structural Characteristics, Reconstruction of Paleoslope and Triggering Mechanism of Slump. *J. Geol. Soc. Korea* **2015**, *51*, 545–560, (In Korean with English abstract). [CrossRef]

19. Byun, U.H.; Van Loon, A.J.T.; Kwon, Y.K.; Ko, K. A New Type of Slumping-Induced Soft-Sediment Deformation Structure: The Envelope Structure. *Geologos* **2019**, *25*, 111–124. [CrossRef]

20. Chough, S.K.; Kwon, S.T.; Ree, J.H.; Choi, D.K. Tectonic and Sedimentary Evolution of the Korean Peninsula: A Review and New View. *Earth Sci. Rev.* **2000**, *52*, 175–235. [CrossRef]

21. Sagong, H.; Kwon, S.-T.; Ree, J.-H. Mesozoic Episodic Magmatism in South Korea and Its Tectonic Implication. *Tectonics* **2005**, *24*, 2004TC001720. [CrossRef]

22. Cho, H.; Son, M.; Cheon, Y.; Sohn, Y.K.; Kim, J.S.; Kang, H.C. Evolution of the Late Cretaceous Dadaepo Basin, SE Korea, in Response to Oblique Subduction of the Proto-Pacific (Izanagi/Kula) or Pacific Plate. *Gondwana Res.* **2016**, *39*, 145–164. [CrossRef]

23. Paik, I.S.; Huh, M.; So, Y.H.; Lee, J.E.; Kim, H.J. Traces of Evaporites in Upper Cretaceous Lacustrine Deposits of Korea: Origin and Paleoenvironmental Implications. *J. Asian Earth Sci.* **2007**, *30*, 93–107. [CrossRef]

24. Kim, S.B.; Chough, S.K.; Chun, S.S. Tectonic Controls on Spatiotemporal Development of Depositional Systems and Generation of Fining-Upward Basin Fills in a Strike-Slip Setting: Kyokpori Formation (Cretaceous). south-west Korea. *Sedimentology* **2003**, *50*, 639–665. [CrossRef]

25. Gihm, Y.S.; Kim, M.; Son, M.; Hwang, I.G. The Influence of Tectonic Subsidence on Volcaniclastic Sedimentation: The Cretaceous Upper Daeri Member, Wido Island, Korea. *Isl. Arc* **2017**, *26*, e12183. [CrossRef]

26. Chun, S.S.; Chough, S.K. Depositional Sequences From High-Concentration Turbidity Currents, Cretaceous Uhangri Formation (SW Korea). *Sediment. Geol.* **1992**, *77*, 225–233. [CrossRef]

27. Gihm, Y.S.; Hwang, I.G. Syneruptive and Intereruptive Lithofacies in Lacustrine Environments: The Cretaceous Beolkeum Member, Wido Island, Korea. *J. Volcanol. Geotherm. Res.* **2014**, *273*, 15–32. [CrossRef]

28. Koh, H.J.; Kwon, C.W.; Park, S.-I.; Park, J.; Kee, W.-S. *Geological Report of the Julpo Sheet (1:50,000). Daejon*; Korea Institute of Geoscience and Mineral Resources: Daejeon, South Korea, 2013; p. 81, (In Korean with English abstract).

29. Choi, S.; Lee, Y.N. Possible Late Cretaceous Dromaeosaurid Eggshells from South Korea: A New Insight Into Dromaeosaurid Oology. *Cret. Res.* **2019**, *103*, 104–167. [CrossRef]

30. Choi, S.; Lee, S.K.; Kim, N.H.; Kim, S.; Lee, Y.N. Raman Spectroscopy Detects Amorphous Carbon in an Enigmatic Egg From the Upper Cretaceous Wido Volcanics of South Korea. *Front. Earth Sci.* **2020**, *7*, 349. [CrossRef]

31. Byun, U.H.; Van Loon, A.J.; Kwon, Y.K.; Ko, K. Intrastratal Flow in the Cretaceous Gyeokpori Formation (SW South Korea). *Geol. Q.* **2020**, *64*, 611–625. [CrossRef]

32. Lee, D.S. On the Geology and Oily Material-Containing Formation in Haenam Area, Jeollanam-do, Korea. *J. Geol. Soc. Korea* **1964**, *1*, 35–49.

33. Lee, D.S.; Lee, H.Y. Geological and Geochemical Study on the Rock Sequences Containing Oily Materials in Southern Coast Area of Korea. *J. Korea Inst. Min. Geol.* **1976**, *9*, 45–74, (In Korean with English abstract).

34. Chough, S.K.; Chun, S.S. Intrastratal Rip-Down Clasts, Late Cretaceous Uhangri Formation, Southwest Korea. *J. Sediment. Res.* **1988**, *58*, 530–533.

35. Chough, S.K.; Kim, S.B.; Chun, S.S. Sandstone/Chert and Laminated Chert/Black Shale Couplets, Cretaceous Uhangri Formation (Southwest Korea): Depositional Events in Alkaline Lake Environments. *Sediment. Geol.* **1996**, *104*, 227–242. [CrossRef]

36. Paces, J.B.; Miller, J.D. Precise U-Pb Ages of Duluth Complex and Related Mafic Intrusions, Northeastern Minnesota: Geochronological Insights to Physical, Petrogenetic, Paleomagnetic, and Tectonomagmatic Processes Associated With the 1.1 Ga Midcontinent Rift System. *J. Geophys. Res.* **1993**, *98*, 13997–14013. [CrossRef]
37. Claoué-Long, J.C.; Compston, W.; Roberts, J.; Fanning, C.M. Two Carboniferous Ages: A Comparison of SHRIMP Zircon Dating With Conventional Zircon Ages and 40Ar/39Ar Analysis. In *Geochronology Time Scales and Global Stratigraphic Correlation*; Berggren, W.A., Kent, D.B., Auberey, M.P., Hardenbol, J., Eds.; S.E.P.M. (Soc. Sediment. Geol.) Spec. Publ: Broken Arrow, OK, USA, 1995; Volume 54, pp. 3–21.
38. Williams, I.S. U-Th-Pb Geochronology by Ion Microprobe. In *Applications of Microanalytical Techniques to Understanding Mineralizing Processes*; Rev. Econ. Geol. McKibben, M.A., Shanks, W.C., III, Ridley, W.L., Eds.; Society of Economic Geologists: Socorro, NJ, USA, 1998; Volume 7, pp. 1–35.
39. Stacey, J.S.; Kramers, J.D. Approximation of Terrestrial Lead Isotope Evolution by a Two-Stage Model. *Earth Planet. Sci. Lett.* **1975**, *26*, 207–221. [CrossRef]
40. Ludwig, K.R. *User's Manual for Isoplot 3.6: A Geochronological Toolkit for Microsoft Excel*; [Berkeley Geochronology Center special publication, 2008]; Berkeley Geochronology Center: Berkeley, CA, USA, 2008.
41. Ludwig, K.R. *User's Manual for SQUID 2*; [Berkeley Geochronology Center special publication, 2009]; Berkeley Geochronology Center: Berkeley, CA, USA, 2009.
42. Manville, V.; Németh, K.; Kano, K. Source to Sink: A Review of Three Decades of Progress in the Understanding of Volcaniclastic Processes, Deposits, and Hazards. *Sediment. Geol.* **2009**, *220*, 136–161. [CrossRef]
43. Major, J.J.; Janda, R.J.; Daag, A.S. Watershed Disturbance and Lahars on the East Side of Mount Pinatubo During the Mid-June 1991 Eruptions. In *Fire and Mud: Eruptions and Lahars of Mount Pinatubo*; Philippines Newhall, C.G., Punongbayan, R.S., Eds.; University of Washington Press: Seattle, WA, USA, 1996; pp. 895–919.
44. Major, J.J.; Pierson, T.C.; Dinehart, R.L.; Costa, J.E. Sediment Yield Following Severe Volcanic Disturbance?—A Two-Decade Perspective From Mount St. Helens. *Geology* **2000**, *28*, 819–822. [CrossRef]
45. Hayes, S.K.; Montgomery, D.R.; Newhall, C.G. Fluvial Sediment Transport and Deposition Following the 1991 Eruption of Mount Pinatubo. *Geomorphology* **2002**, *45*, 211–224. [CrossRef]
46. Paik, I.S.; Kim, H.J. Playa Lake and Sheetflood Deposits of the Upper Cretaceous Jindong Formation, Korea: Occurrences and Palaeoenvironments. *Sediment. Geol.* **2006**, *187*, 83–103. [CrossRef]
47. Pearce, J.A.; Harris, N.B.W.; Tindle, A.G. Trace Element Discrimination Diagrams for the Tectonic Interpretation of Granitic Rocks. *J. Petrol.* **1984**, *25*, 956–983. [CrossRef]
48. Nilsen, T.H.; Sylvester, A.G. Strike-Slip Basins. In *Tectonics of Sedimentary Basins*; Busby, C.J., Ingersoll, R.V., Eds.; Blackwell Publishing Science: Cambridge, MA, USA, 1995; pp. 425–457.
49. Lee, T.-H.; Park, K.-H.; Yi, K.; Geng, J.; Li, H. 2015, SHRIMP U-Pb ages and Hf isotopic composition of the detrital zircons from the Myogok Formation, SE Korea: Development of terrestrial basin and igneous activity during the early Cretaceous. *Geosci. J.* **2015**, *19*, 189–203. [CrossRef]
50. Lee, T.-H.; Park, K.-H.; Yi, K. SHRIMP U-Pb ages of detrital zircons from the Early Cretaceous Nakdong Formation, South East Korea: Timing of initiation of the Gyeongsang Basin and its provenance. *Isl. Arc* **2018**, *27*, e12258. [CrossRef]
51. Lee, T.-H.; Park, K.-H.; Yi, K. Nature and evolution of the Cretaceous basins in the eastern margin of Eurasia: A case study of the Gyeongsang Basin, SE Korea. *J. Asian Earth Sci.* **2018**, *166*, 19–31. [CrossRef]